BULLETIN

Feature Article

Frit-Inlet Asymmetrical Flow Field-Flow Fractionation (FI-AFlFFF): A Stopless Separation Technique for Macromolecules and Nanoparticles

Myeong Hee Moon

Department of Chemistry and Chemistry Institute for Functional Materials,
Pusan National University, Pusan 609-735, Korea
Received February 27, 2001

This article gives an overview of a recently developed channel system, frit-inlet asymmetrical flow field-flow fractionation (FI-AFlFFF), which can be applied for the separation of nanoparticles, proteins, and water soluble polymers. A conventional asymmetrical flow FFF channel has been modified into a frit-inlet asymmetrical type by introducing a small inlet frit near the injection point and the system operation of the FI-AFlFFF channel can be made with a great convenience. Since sample components injected into the FI-AFlFFF channel are hydro-dynamically relaxed, sample injection and separation processes proceed without interruption of the migration flow. Therefore in FI-AFlFFF, there is no requirement for a valve operation to switch the direction of the migration flow that is normally achieved during the focusing/relaxation process in a conventional asymmetrical channel. In this report, principles of the hydrodynamic relaxation in FI-AFlFFF channel are described with equations to predict the retention time and to calculate the complicated flow variations in the developed channel. The retention and resolving power of FI-AFlFFF system are demonstrated with standard nanospheres and protreins. An attempt to elucidate the capability of FI-AFlFFF system for the separation and size characterization of nanoparticles is made with a fumed silica particle sample. In FI-AFlFFF, field programming can be easily applied to improve separation speed and resolution for a highly retaining component (very large MW) by using flow circulation method. Programmed FI-AFlFFF separations are demonstrated with polystyrene sulfonate standards and pululans and the dynamic separation range of molecular weight is successfully expanded.

Keywords : Flow field-flow fractionation, Frit-inlet asymmetrical channel, Nanoparticle separation.

Introduction

Field-flow fractionation (FFF) is a group of separation techniques applicable to the separation and characterization of macromolecules and particulate materials ranging from nanosized to supramicron sized.[1,2] Since the field-flow fractionation concept was first introduced by Giddings in 1966,[3] it has been diversified into a number of subtechniques along with theoretical developments. Generally, FFF is an elution technique fractionating sample components according to their diffusivity and mobility which are closely related to molecular weight or particle size. Separation in FFF is carried out in a thin flat channel with a rectangular cross sec-

tion.[4,5] The simple configuration of an FFF channel is illustrated as shown in Figure 1 with an external field imposed perpendicular to the direction of channel flow and a parabolic flow profile which provides different flow velocities across the channel thickness. The external field in FFF plays a crucial role in partitioning sample components with different diffusions into flow streamlines of differing velocities. The differential distribution of sample components across the channel results in differing migrations of each component due to their different flow velocities of the parabolic flow streamlines.

Flow FFF, one of the subtechniques of the FFF family, utilizes a secondary flow as an external field and it becomes a
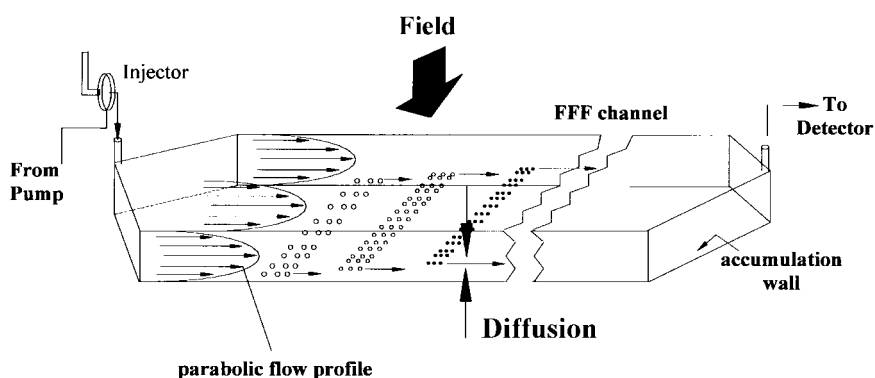
Figure 1. Schematic diagram showing parabolic flow streamlines in a rectangular FFF channel. Real sample bands should be more like a distributed form of sample clouds though they appear as discrete sample layers in the diagram.

universal technique due to the wide size range of sample applications from 1 nm to about 50 μm, which includes nanoparticles, colloids, proteins, and water soluble polymers.[6-8] In flow FFF, a secondary flow, the so-called crossflow, is driven from one of the channel walls toward the other wall. Both walls are made of porous ceramic frit and the field strength can be varied by controlling the rate of crossflow. The channel wall towards which crossflow is driven is called an accumulation wall, and is normally overlaid with a semipermeable membrane to prevent the passage of sample materials. A sample component in flow FFF channel experiences a drag of crossflow and simultaneously exhibits a diffusive motion against the wall. The two opposite transports of a sample component in flow FFF channel are balanced at a certain equilibrium height from the accumulation wall and the equilibrium locations are largely governed by the difference in diffusion coefficients of sample components. Therefore, particles or macromolecules of a smaller Stoke's diameter having a faster diffusion protrude toward the high speed flow streamlines than those with larger diameters and the particles are separated according to increasing particle diameter.

The conventional flow FFF channel has a symmetrical assembly in which there are two permeable walls and the crossflow rate is normally adjusted to be the same as the incoming flow rate at the depletion wall (opposite from accumulation wall).[9,10] Thus, there are two different flow streams entering into and exiting the channel. In Figure 2a, the side view of symmetrical flow FFF channel is illustrated. Later, the flow FFF channel system has been operated without the permeable depletion wall and this is termed an asymmetrical channel.[11,12] The asymmetrical type of channel was also developed by replacing depletion wall with a glass plate as shown in Figure 2b. In an asymmetrical flow FFF channel, there is no input of crossflow, but the crossflow field can be generated by allowing the flow to penetrate through the accumulation wall. In this channel, crossflow is provided by the part of channel flow that is pumped from the channel inlet and the remaining flow exits through the channel outlet by carrying sample components.

However for both flow FFF channels, sample materials must be driven to their equilibrium positions before their longitudinal migration begins. This is the relaxation process, which is a pre-requisite step to establish a steady state distribution of sample components across the channel. In case of a symmetrical channel, relaxation is achieved by stopping channel flow (longitudinal direction) for a certain period of time right after sample injection while crossflow is applied to the channel.[4,10] During the relaxation process, channel flow bypasses the channel and this is illustrated as a bold line at the simple side view of a symmetrical flow FFF channel in Figure 2a. Figure 2 shows the configuration of flow directions during the relaxation process for three different flow FFF channels. The stop-flow process in the conventional symmetrical channel is an important procedure since it greatly reduces the spreading of an initial sample band. After the relaxation process is completed, channel flow is resumed in order to initiate the separation process. In an asymmetrical flow FFF channel, sample relaxation is achieved in a different way since there is no flux from the depletion wall. Thus, relaxation of sample components in this channel is allowed to occur below the injection point by focusing the two counter-directing flow streams originated from both the channel inlet and the outlet as shown in Figure 2b.[12,13] Note that the injection point is apart from the channel inlet. After the focusing/relaxation, flow moving from the channel outlet toward the focusing point is reversed so that it flows toward the channel inlet and the separation process begins. Since the focusing/relaxation process is expected to compress an injected sample cloud into a narrow band by the two counter-directing flows, band broadening of an eluted peak can successfully be reduced to a good extent. In addition, migrating sample bands are somehow compressed longitudinally during migration along the channel since the linear flow velocity decreases along channel axis due to the loss of crossflow. From a mechanical point of view, flow penetration through a ceramic frit can not be uniform due to the irregular spacing of the locations of the pores along the surface of the ceramic frit. Thus, an asymmetrical flow FFF channel utilizing only one permeable frit may reduce the non-ideal phenomenon of crossflow passage and this will reduce the broadening of a final peak. For all of these reasons, it is known through experiments that an asymmetrical flow FFF channel provides a better resolution in separation
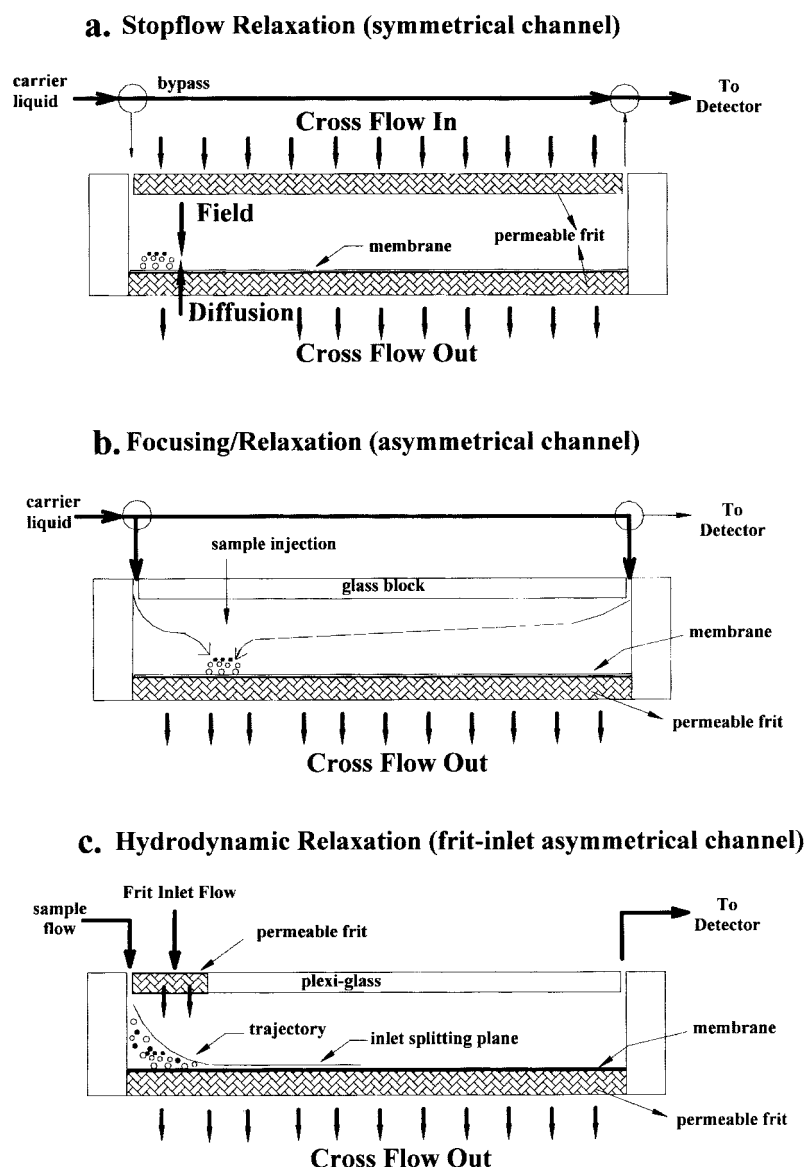
a. **Stopflow Relaxation (symmetrical channel)**

b. **Focusing/Relaxation (asymmetrical channel)**

c. **Hydrodynamic Relaxation (frit-inlet asymmetrical channel)**

Figure 2. Side views of three different flow FFF channels (a. symmetrical, b. asymmetrical, c. frit-inlet asymmetrical channel) showing the flow direction during sample relaxation (bold lines) and during separation (solid lines).

than a symmetrical channel.

However, both relaxation techniques are based on the temporary stoppage of longitudinal migration of sample materials. During this period, sample components are forced by crossflow toward the accumulation wall that is covered by a semipermeable membrane. Occasionally, some particles are adsorbed by the channel membrane. When flow is resumed after the relaxation processes, an abrupt change in the flow stream causes a sudden increase in or a release of system pressure leading to a baseline shift in the detector signal. The pressure change may also disturb the steady state equilibrium of the relaxed sample materials and this may result in a sweep of some of sample materials along with void peak or in an early elution. For all of these reasons, it is desirable to bypass the static relaxation process if sample relaxation can be somehow provided. As an alternative to these relaxation procedures, a hydrodynamic relaxation process was pro-

posed with both frit-inlet and split inlet channel systems.[14-16] In the hydrodynamic relaxation method, sample materials are introduced to channel inlet with a relatively low flow rate and a large amount of channel flow is introduced through a small inlet frit placed near the injection point of the depletion wall. When the two flow streams merge together, sample components are driven toward the accumulation wall by the relatively fast frit flow, where they can reach their steady state equilibrium hydrodynamically within the inlet frit region. When sample materials leave the relaxation segment, they enter the separation segment and separation begins smoothly. When the frit inlet concept is utilized in a symmetrical channel, manipulating the sample flow, frit flow, and crossflow is required. In order to have a successful hydrodynamic relaxation to occur, frit flow must be approximately 20 times faster than the sample flow. In this case, the summation of sample stream and frit inlet stream becomes

the total axial flow (channel outlet flow) and the combined flow becomes a considerable amount. Therefore, the ability to manipulate the lowest axial flow rate is limited. Consequently, to retain low retaining sample components in the channel an even higher crossflow speed is required. The subsequent increase in crossflow rate is needed to compensate for the increase of the axial flow rate and this is critical to the channel wall material (ceramic frit plate) in flow FFF. In addition, increased axial flow rate requires an increase in the injection amount of sample materials for them to be detected. From these reasons, hydrodynamic relaxation has not been further developed in flow FFF.

Recently, the hydrodynamic relaxation method using the frit-inlet concept was applied to an asymmetrical flow FFF channel and the frit-inlet asymmetrical flow FFF (FI-AFlFFF) system has been under developed.[17-20] The inlet frit element is placed near the inlet of the depletion wall of an asymmetrical channel and the sample injection is injected directly into the flowing streamlines. Figure 2c illustrates particle trajectory that can expected to result from an asymmetrical channel using a hydrodynamic relaxation method. The schematic view of the frit-inlet asymmetrical flow channel is plotted in Figure 3. FI-AFlFFF system is advantageous because the stopless flow operation removes all of the complicated devices such as valves and tees for flow conversion. In addition, it bypasses a temporary stoppage of sample migration, which often results in adsorption of sample materials onto channel membrane. Once a hydrodynamic relaxation is successfully achieved, separation process in FI-AFlFFF channel is similar to that of a conventional asymmetrical channel that provides a high resolution separation. From the initial evaluation of FI-AFlFFF for the separation of standard particles and proteins, it has been found that hydrodynamic relaxation can successfully be achieved at about a 5 : 95 ratio of sample flow to frit flow rate.[17,18] Theoretical calculations for the variation of flow velocities were accomplished to predict retention time at frit inlet asymmetrical channel and the results showed that the retention in FI-AFlFFF channel basically follows the general principles of field-flow fractionation.[19]

In this article, principles of frit-inlet asymmetrical flow FFF separation are explained with the theory related with the calculation of diffusion coefficient or hydrodynamic diameter of sample components from experimental retention time. The separation capability of FI-AFlFFF is demonstrated with latex spheres, nanosized fumed silica, proteins, and water soluble polymeric standards. A recent improvement[20] for a separation of broad MW ranges of polystyrene sulfonates with resolution enhancement is also discussed by introducing the field programming method into a frit-inlet asymmetrical flow FFF system.

Theory

Retention in FI-AFlFFF Channel. In frit-inlet asymmetrical flow FFF channel, sample relaxation and separation are continuously achieved right after the sample injection.

As it is shown in Figure 2c, injected sample materials are compressed toward the accumulation wall by the relatively high speed frit flow and simultaneously they are longitudinally transported down the channel. Once they reach the end of the inlet frit element, they are expected to attain their equilibrium heights depending upon their diffusivity and are smoothly transferred to the separation segment for migrations. Retention in the separation segment is expected to be similar to that observed in conventional flow FFF channel system if the hydrodynamic relaxation is successfully achieved. Retention in frit-inlet asymmetrical flow FFF channel follows the basic principle of FFF as known by the retention ratio, R, which is the ratio of channel void time, t^0, to retention time, t_r, given by[2,21]

$$R = \frac{t^0}{t_r} = 6\lambda\left(\coth\frac{1}{2\lambda} - 2\lambda\right) \qquad (1)$$

where λ is the dimensionless parameter representing the fractional height of a sample band at equilibrium within the channel as expressed by the ratio of mean layer thickness, l, to channel thickness, w. For a sufficiently long retained component, λ becomes very small and the right side of equation 1 can be simplified as $R \cong 6\lambda$. The mean layer thickness, the average height of a sample band, is closely related to the field strength (scaled by crossflow velocity, U) and the diffusion coefficient, D, of sample material as

$$l = \frac{D}{U} \qquad \left(D = \frac{kT}{3\pi\eta d_s}\right) \qquad (2)$$

where kT is thermal energy, η is the viscosity of the carrier liquid, and d_s is the Stokes diameter of sample component. Therefore, retention time in a simplified form can be calculated as a function of diffusion coefficient by rearranging equation 2 into 1 as

$$t_r \cong \frac{t^0}{6\lambda} = \frac{\dot{V}_c w^2}{6DV^0}t^0 \qquad (3)$$

It is shown in equations 2 and 3 that retention time increases as hydrodynamic diameter of sample components (small diffusion coefficient) and crossflow rate $\dot{V}_c$ increase. The volumetric flow rate of crossflow $\dot{V}_c$ is related with crossflow velocity as $\dot{V}_c = bLU$, where b is the breadth of the channel. The above equation is valid for flow FFF channels (symmetrical and asymmetrical) except for those that use a cylindrical channel as such as hollow fiber flow FFF (R for HF-FlFFF is approximately 4λ) once void time is properly calculated.[22,23]

The void time, t^0, in a conventional symmetrical channel is simply calculated by dividing the channel length, L, by the average velocity of migration flow, $\langle v \rangle (= \dot{V}/bw)$, where $\dot{V}$ is the volumetric flow rate of channel flow. However, migration flow velocity in frit-inlet asymmetrical channel varies through the entire channel length since sample flow and frit flow are mixed at the relaxation segment and simultaneously, part of these flows are lost through the accumula-
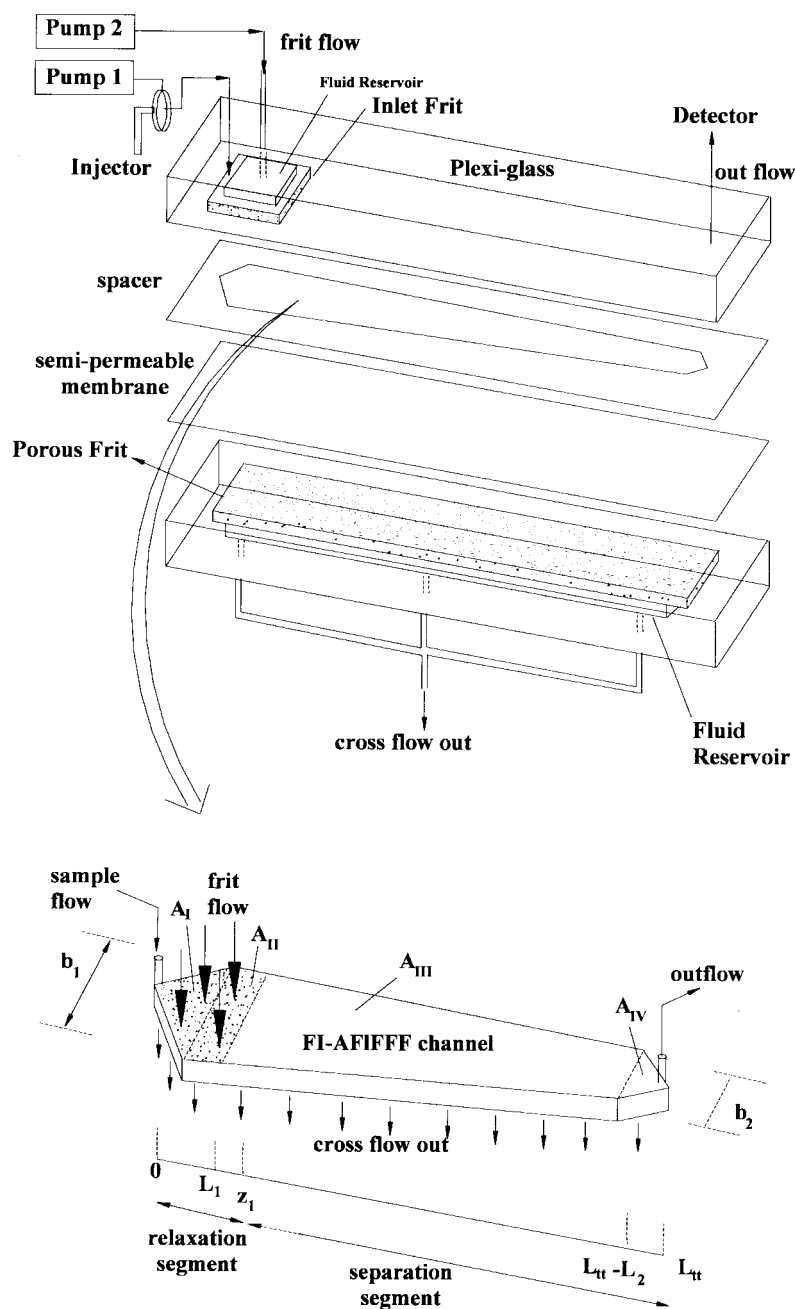
Figure 3. Schematic illustration of channel assembly of the frit-inlet asymmetrical flow FFF (FI-AFlFFF) channel. Trapezoidal geometry of channel is enlarged with the two inlet flows (sample and frit flow) and the two outlet flows (crossflow and outflow).

tion wall by crossflow. Therefore, calculation of void time in FI-AFlFFF channel is considered with the variable flow velocities along the channel axis z as[19]

$$t^0 = \int_0^L \frac{dz}{\langle v \rangle(z)} \tag{4}$$

Since the channel flow rate varies along the channel axis, z, in frit-inlet asymmetrical channel, mean flow velocity varies together. When the channel breadth varies as in trapezoidal channel such as those shown in Figure 3, the variation of mean flow velocity is separately considered within the four successive channel segments, *I~IV*, and it can be expressed as follows.[19]

$$\langle v \rangle_I(z) = \frac{\dot{V}_s + (\dot{V}_f/V_f - \dot{V}_c/A_c)A_I(z)}{wb_I(z)} \tag{5}$$

$$\langle v \rangle_{II}(z) = \frac{\dot{V}_s + (\dot{V}_f/V_f - \dot{V}_c/A_c)(A_I(L_1) + A_{II}(z))}{wb_{II}(z)} \tag{6}$$

$$\langle v \rangle_{III}(z) = \frac{\dot{V}_s + \dot{V}_f - \dot{V}_c(A_f + A_{III}(z))/A_c}{wb_{III}(z)} \tag{7}$$

$$\langle v \rangle_{IV}(z) = \frac{\dot{V}_s + \dot{V}_f - \dot{V}_c(A_f + A_{III}(L_{tt} - L_2) + A_{IV}(z))/A_c}{wb_{IV}(z)} \tag{8}$$

where the subscript *s*, *f*, *c*, and *out* for the volumetric flow

Table 1. The variable breadth and area of the four channel segments along the channel axis, z, in frit-inlet asymmetrical flow FFF channel

segment	$b(z)$	$A(z)$	limits
I	$\dfrac{b_1}{L_1}z$	$\dfrac{b_1}{2L_1}z^2$	$(0 \leq z \leq L_1)$
II		$b_1(z-L_1)-\dfrac{b_1-b_2}{L_{tt}-L_1-L_2}\dfrac{(z-L_1)^2}{2}$	$(L_1 \leq z \leq z_1)$
III	$b_1-\dfrac{b_1-b_2}{L_{tt}-L_1-L_2}(z-L_1)$	$b_1(z-L_1)-\dfrac{b_1-b_2}{L_{tt}-L_1-L_2}\left\{\dfrac{(z-L_1)^2}{2}-\dfrac{(z_1-L_1)^2}{2}\right\}$	$(z_1 \leq z \leq L_{tt}-L_2)$
IV	$\dfrac{b_2}{L_2}(L_{tt}-z)$	$\dfrac{b_2}{2L_2}\{L_2^2-(L_{tt}-z)^2\}$	$(L_{tt} \leq L_2 \leq z-L_{tt})$

rate term as $\dot{V}_s$, $\dot{V}_f$, $\dot{V}_c$, and $\dot{V}_{out}$ represent the sample flow, frit flow, crossflow, and outflow, respectively and L_1 the length of triangular endpiece of inlet, L_2 for the outlet, and L_{tt} for the tip-to-tip channel length. The variable area within each segment, $A_I(z)\sim A_{IV}(z)$, and the variable channel breadths, $b_I(z)\sim b_{IV}(z)$ are listed in Table 1. A_f and A_c are the area of the inlet frit element and of the accumulation wall, respectively, and are expressed as[19]

$$A_f = \frac{b_1 L_1}{2}+b_1(z_1-L_1)-\frac{b_1-b_2}{L_{tt}-L_1-L_2}\frac{(z_1-L_1)^2}{2} \qquad (9)$$

$$A_c = \frac{1}{2}\{b_1(L_{tt}-L_2)+b_2(L_{tt}-L_1)\} \qquad (10)$$

where z_1 is the length of inlet frit element, b_1 and b_2 are the breadths of the inlet and the outlet, respectively. Once the channel flow rate conditions are determined, then channel flow velocity expressions in Equations 5-8 can be calculated experimentally using the known channel dimension. The equations 5-10 are valid for both rectangular (same breadth throughout the channel) and trapezoidal (decreasing channel breadth as shown in Figure 3) channels.

The void time throughout the frit-inlet asymmetrical channel is the summation of passage time within each segment that is calculated by integrating the inverse of mean flow velocity as

$$t^0 = \int_0^{L_1} \frac{dz}{\langle v \rangle_I(z)} + \int_{L_1}^{z_1} \frac{dz}{\langle v \rangle_{II}(z)} + \int_{z_1}^{L_{tt}-L_2} \frac{dz}{\langle v \rangle_{III}(z)}+$$

$$\int_{L_{tt}-L_2}^{L_{tt}} \frac{dz}{\langle v \rangle_{IV}(z)} \qquad (11)$$

and the total void time is found by substituting equations 5-10 into equation 11 as

$$t^0 = \frac{V^0 A_f/A_c}{(\dot{V}_f-\dot{V}_c A_f/A_c)}\ln\left(\frac{\dot{V}_s+\dot{V}_f-\dot{V}_c A_f/A_c}{\dot{V}_s}\right)+\frac{V^0}{\dot{V}_c}\ln$$

$$\left(\frac{\dot{V}_s+\dot{V}_f-\dot{V}_c A_f/A_c}{\dot{V}_{out}}\right) \qquad (12)$$

where V^0 is the void volume of the channel. Equation 12 is

valid when $\dot{V}_f/A_f > \dot{V}_c/A_c$. Equation 12 is now expressed with experimental flow rates, the geometrical area of the inlet frit, and the accumulation wall as expressed in Table 1. It is applicable to both rectangular and trapezoidal channel geometries. From equation 12, we can calculate the effective channel flow rate of FI-AFlFFF, which is the channel flow rate equivalent to a symmetrical flow FFF channel, as

$$\dot{V}_{eff} = \left\{\frac{A_f/A_c}{(\dot{V}_f-\dot{V}_c A_f/A_c)}\ln\left(\frac{\dot{V}_s+\dot{V}_f-\dot{V}_c A_f/A_c}{\dot{V}_s}\right)+\frac{1}{\dot{V}_c}\ln\right.$$

$$\left.\left(\frac{\dot{V}_s+\dot{V}_f-\dot{V}_c A_f/A_c}{\dot{V}_{out}}\right)\right\}^{-1} \qquad (13)$$

When the hydrodynamic relaxation of sample components is achieved quickly under a high speed frit flow (normally 20 times faster than the sample flow), the amount of time devoted to relaxation out of the total retention time is assumed to be very small and the retention time in FI-AFlFFF channel can be approximated by substituting equation 12 into equation 3 as

$$t_r = \frac{w^2}{6D}\left\{\frac{1}{\left(\dfrac{\dot{V}_f/A_f}{\dot{V}_c/A_c}-1\right)}\ln\left(\frac{\dot{V}_s+\dot{V}_f-\dot{V}_c A_f/A_c}{\dot{V}_s}\right)+\ln\right.$$

$$\left.\left(\frac{\dot{V}_s+\dot{V}_f-\dot{V}_c A_f/A_c}{\dot{V}_{out}}\right)\right\} \qquad (14)$$

Equation 14 shows that retention time in FI-AFlFFF is inversely proportional to the diffusion coefficient or it is proportional to a hydrodynamic diameter of sample components. Practically, equation 14 can be used to calculate the diffusion coefficient or the diameter of a sample component from experimentally observed retention time and to obtain particle size distribution of a polydispersed particulate sample from an experimental fractogram. Equation 14 applies to the calculation of a strongly retained sample component. However in case of moderate retention, full equations as expressed in the right hand side of equation 1 must be used

for the calculation of retention time (equation 3) instead of using the approximated form of retention ratio ($R = 6\lambda$) as used in equation 14.

Field Programming in FI-AFlFFF. In field-flow fractionation, programming techniques are often used to hasten the elution of highly retained sample components (larger particles) by decaying the field strength during separation.[24-26] Field decay is the most common programming technique used in sedimentation FFF and thermal FFF.[24,27,28] In addition to the decrease in separation time, an increase in the detectability of strongly retained components is an advantage of using field programming.[29,30] Field programming in Flow FFF can also be achieved by varying the crossflow rate during its operation but it has not been widely employed except in a few attempts[31] since it is difficult to maintain consistent channel flow velocity during field (crossflow) programming in a channel having two different flow exits (channel out and crossflow out).

Field programming has been recently applied to an FI-AFlFFF system and shown to be powerful in separating a wide MW range of water soluble polymers.[20] It can be achieved by connecting the crossflow out to the pump inlet for the frit flow and then varying the rate of circulating flow. When the flow circulation is employed in FI-AFlFFF channel, flow rate of cross out is the same as the frit flow rate during programming. The operation of the system becomes more versatile when the programming technique is applied to the FI-AFlFFF channel system since sample injection, relaxation, and separation are in continuous operation and do not interrupt the migration flow.

Field programming can be used with linear, exponential, power decay.[29-32] While the linear decay is the simplest form of decay pattern, the latter is widely used in FFF technologies since it provides a uniform fractionating power over wide ranges of particle diameter during field programming. The decay patterns are operated while holding the initial field strength constant for a period of time, t_1, and then the field decays following the different patterns illustrated in Figure 4. The linear field decay is expressed as follows[20]
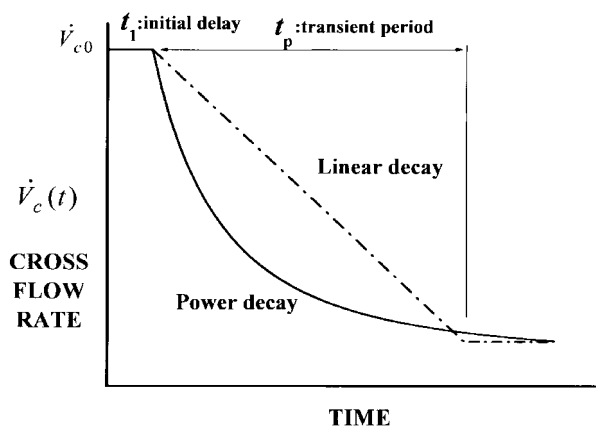

Figure 4. Linear decay (broken line) and power decay (solid line) in field programming. t_1: initial delay time, t_p: transient time.

$$\dot{V}_c(t) = \dot{V}_{c0} - \Delta \dot{V}_c \left(\frac{t - t_1}{t_p} \right) \qquad (t_1 \le t \le t_1 + t_p) \qquad (15)$$

where $\dot{V}_c(t)$ is the crossflow rate at time t, t_1 is the initial time delay, t_p is the transient time for programming, $\dot{V}_{c0}$ is the initial crossflow rate, and $\Delta \dot{V}_c$ is the decrease in crossflow rates during the programming. For $t < t_1$, $\dot{V}_c(t)$ is fixed at the initial flow rate of $\dot{V}_{c0}$, and for $t > t_1 + t_p$, $\dot{V}_c(t)$ is equal to $\dot{V}_{c0} - \Delta \dot{V}_c$. Field strength in power programming is held constant for a period of initial delay, t_1, and then programmed according to the equation

$$\dot{V}_c(t) = \dot{V}_{c0} \left(\frac{t_1 - t_a}{t - t_a} \right)^p \qquad (16)$$

where t_a is a time parameter ($t_a = -pt_1$) and p is a power equivalent to 2 which is known to provide a uniform fractionating power in flow FFF.

Programming in FI-AFlFFF can also be integrated to a dual mode by adding the ramping of migration flow while the field strength is decaying. By utilizing dual field and flow programming, separation of a broad MW range of polymeric materials can be fastened more efficiently and the sample recovery of such highly retaining materials can also be improved.

Experimental Methods

The frit-inlet asymmetrical flow FFF channel system is built in-house with two plexi-glass blocks (5-cm thick) as illustrated Figure 3. The frit elements used for FI-AFlFFF channel are porous ceramic made of alumina and they are obtained from FFFractionation, LLC (Salt Lake City, UT, USA). The channel spacer is a Mylar sheet and is cut in a ribbonlike shape as shown in Figure 3. The channel is 27.2 cm long for tip-to-tip. Three different channels are employed for this work and they are different in thicknesss (127, 178, and 254 μm for channels I~III, respectively). Channel I is rectangular having a constant breadth of 2.0 cm and the other two are trapezoidal with the initial breadth of 2.0 cm and a final breadth of 1.0 cm at the tapered end. The length of the frit inlet element is 3.1 cm from the channel inlet. The membrane used for the accumulation wall is regenerated cellulose having MW cut-off of 10,000 from Millipore Corp. (Bedford, MA, USA).

Particle samples are polystyrene latex standards having nominal diameters of 20, 50, 93, 135, and 222 nm from Duke Scientific Co. (Palo Alto, CA, USA) and a fumed silica from Sigma (St. Louis, MO, USA). Proteins are cytochrome-C (12.4 K), carbonic anhydrase (29 K), BSA (66 K), alcohol dehydrogenase (150 K), apoferritin (444 K), and thyroglobulin (669 K) from Sigma. Water soluble polymers used are polystyrene sulfonate standards having MW's of 4 K, 30 K, 166 K, 350 K, and 1,000 K, from American Polymer Standards Corp. (Mentor, OH, USA) and pullulan standards of P20 (Mw =22.8 K), P100 (Mw=112 K), and P800 (Mw=788 K) (Shodex Standards, Showa Denko, Tokyo, Japan).

All carrier solutions are prepared with deionized water (>18 MΩ). For the separation of polystyrene latex beads and fumed silica, 0.05% FL-70 is added to maintain particle dispersion with 0.02% NaN$_3$ as a bactericide. When proteins and water soluble polymers are separated, 0.1 M Tris-HCl buffer solution (pH=7.8) is used throughout. In every case the carrier solutions are filtered through a membrane filter (0.45 μm pore size) prior to use.

For the delivery of carrier solutions to FI-AFlFFF channel, two programmable HPLC pumps are utilized: a Dynamax model SD-200 from Rainin Instrument Co. Inc. (Woburn, MA, USA) and a M930 HPLC pump from Young-Lin Co. (Seoul, Korea). Injections were made with a model 7125 loop injector from Rheodyne (Cotati, CA, USA) having a 20 μL loop. The sample amounts for injection are about 1-2 μg for PS standards, about 40 μg for the fumed silica, 2-3 μg for each type of protein, 4-7 μg for each PSS standard, and 2-9 μg for each pullulan. Eluted sample materials are monitored by an M720 UV detector from Young-Lin for particles by a model 410 Differential Refractometer from Waters (Milford, MA, USA) for polystyrene sulfonates and pullulans. The detection of particles and proteins are made at 254 and 280 nm, respectively. Experimental fractograms are saved by a pc with AutochroWin data acquisition program from Young-Lin.

Results and Discussion

In the frit-inlet asymmetrical flow FFF channel, linear channel flow velocities vary along channel axis as shown in equations 5-8 due to the loss of flow through the accumulation wall. For a typical asymmetrical channel with a rectangular geometry having a fixed channel breadth, mean flow velocity will continuously decrease from the inlet toward the end of the channel. When the channel breadth decreases with z (channel axis) as in a trapezoidal design, the decrease of flow velocity along the channel axis is compensated to some degree by the reduction of the channel breadth. In an FI-AFlFFF channel, flow velocity variations within the relaxation segment are complicated due to the influx of frit flow but those within the separation segment are similar to that observed in a conventional asymmetrical channel. Figure 5 shows the calculated patterns for flow velocities by using equations 5-8 as for the two channel geometries of typical channel dimensions: rectangular $b_1=b_2$=2.0 cm, $L_1=L_2$=2.0 cm, L_{tt}=27.2 cm, and w=78.3 μm; trapezoidal b_1=2.0 cm, b_2=1.0 cm, L_1=2.0 cm, L_2=1.0 cm with all the others the same with rectangular channel. Flow rate conditions used for the calculations in Figure 5 are based on $\dot{V}_s/\dot{V}_f$=0.15/2.4 mL/min. and $\dot{V}_{out}/\dot{V}_c$=0.86/1.69 mL/min. The flow velocity at the inlet end of both channels starts with a steep decrease for a very short distance and then increases towards the end of the frit inlet segment due to the influx of frit flow. Since the variation in channel breadth of a trapezoidal channel within the frit-inlet segment is not significantly different from that of the rectangular channel in Figure 5, flow velocities for the two channel geometries appear to be nearly the same. However after the point $z=z_1$ (end of frit-inlet seg-
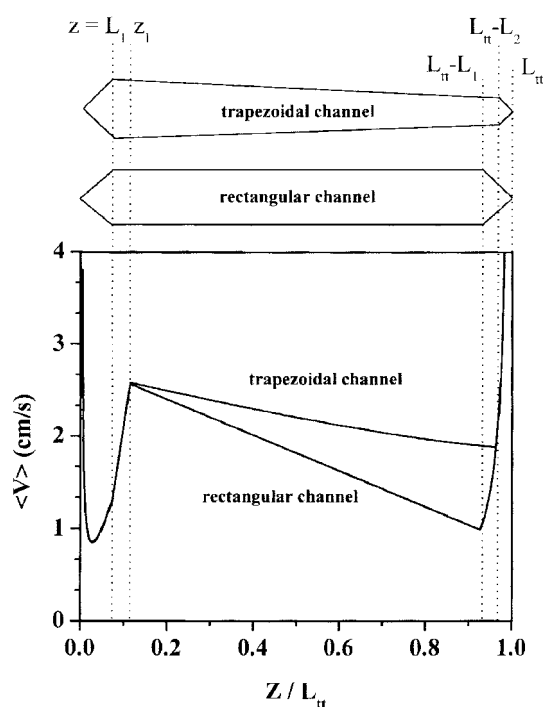

Figure 5. Comparison of linear flow velocities in trapezoidal and rectangular channels. Flow rate conditions are $\dot{V}_s$ = 0.15, $\dot{V}_f$ = 2.4, $\dot{V}_c$ = 1.69, and $\dot{V}_{out}$ = 0.86 mL/min. The channel dimensions used for calculation: Trapezoidal L_1 = 2.0, L_2 = 1.0, b_1 = 2.0, b_2 = 1.0, z_1 = 3.1, L_{tt} = 27.2 cm, and w = 78.3 mm; Rectangular $L_1 = L_2$ = 2.0 cm and $b_1 = b_2$ = 2.0 cm with all other dimensions as for trapezoidal channel. [Reprinted with permission from *Anal. Chem.* **1997**, 69(7) 1438. Copyright 1997 American Chemical Society]

ment), the linear flow velocities start decreasing due to the loss of flow through the accumulation wall of a channel and the variation in the velocities along the rectangular channel (the lower curve) is shown to be more severe than that in the trapezoidal channel (the upper curve). Finally, the steep increase of velocity is begun at the endpiece of both channels toward the channel outlets. In the case of the trapezoidal channel, the significant decrease of migration flow velocity can be reduced by the decrease of channel breadth and this will reduce the retention time of strongly retained materials with a substantial reduction of peak broadening.

In a frit-inlet asymmetrical flow FFF channel, the hydrodynamic relaxation of sample components must be successfully accomplished before the separation process begins. During the hydrodynamic relaxation, sample components are driven under the inlet splitting plane by frit flow and they will reach their equilibrium positions by the balance of the two opposing forces (field strength toward the wall and diffusive transports against the wall). For a hydrodynamic relaxation to be successfully achieved within the short distance of migration from the channel inlet, frit flow rate must be very high compared to the sample feed rate. In addition, the initial width of a sample band must be minimized since it plays an important role in determining the efficiency of separation in FFF systems as well as in any chromatographic system. The initial band width during hydrodynamic relaxation in FI-AFlFFF channel is proportional to the ratio of
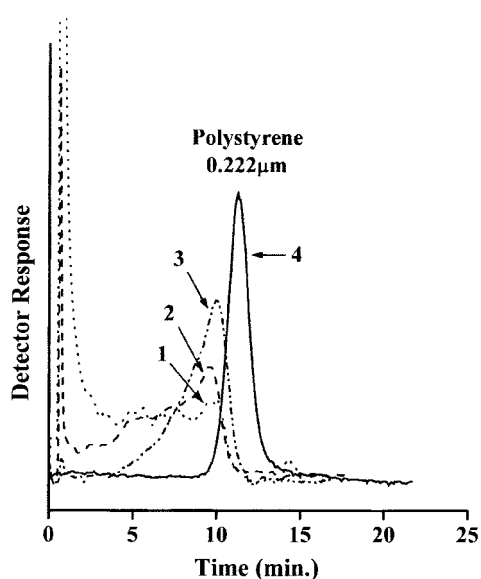
Figure 6. Effect of defferent levels of hydrodynamic relaxation on elution profiles of 0.222 mm latex beads obtained by frit-inlet asymmetrical flow FFF channel. The $\dot{V}_s/\dot{V}_f$ ratios of each profile corresponds to (1) 100/0, (2) 50/50, (3) 30/70, and (4) 6/94, with total inlet flow rate ($\dot{V}_s+\dot{V}_f$) of 1.64 mL/min. All runs are made at $\dot{V}_c = 1.09$, and $\dot{V}_{out} = 0.55$ mL/min. [Reprinted with permission from *Anal. Chem.* **1999**, 71(14) 2661. Copyright 1999 American Chemical Society]

sample stream flow rate to the frit flow rate, $\dot{V}_s/\dot{V}_f$. The dependence of the ratio $\dot{V}_s/\dot{V}_f$ on the sample relaxation can be demonstrated with the examination of elution profiles of standard latex spheres as shown in Figure 6. A polystyrene latex standard of 0.222 μm in diameter is injected at four different levels of the hydrodynamic relaxation by varying the ratio $\dot{V}_s/\dot{V}_f$ as 1) 100/0, 2) 50/50, 3) 30/70, and 4) 6/94. All runs are made using the same channel outflow rate of $\dot{V}_{out} = 0.55$ mL/min. and the crossflow rate of $\dot{V}_c = 1.09$ mL/min. The sum of the two outgoing flow rates ($\dot{V}_{out}+\dot{V}_c$) is identical to the total inlet flow rate through both the channel inlet and frit inlet ($\dot{V}_s+\dot{V}_f$). When there is no frit flow input as shown in run 1 ($\dot{V}_s/\dot{V}_f = 100/0$), hydrodynamic relaxation will not occur and the result shown in the fractogram 1 in Figure 6 appears to be a broad peak that could be observed in a stopless injection at an FFF system. Fractogram 1 is a typical output of a sample injection when a proper relaxation is not provided. When the ratio is decreased to 50/50, the sharp void peak, which is expected to sweep the polystyrene particles right after the beginning of the separation, becomes small. It is further reduced at the ratio 30/70 with the presence of an isolated peak in run 3. The fronting in peak 3 means that part of the latex particles are not completely relaxed during hydrodynamic relaxation due to the weak compression of frit flow. The observed broadening and asymmetry in eluted peak are removed when a much stronger compression of frit flow is used with the ratio 6/94 (0.10/1.54 mL/min. in real flow rates) in run 4. In Figure 6, it is clearly shown that the band broadening caused by the relaxational process can be substantially reduced if a sufficiently small rate of $\dot{V}_s/\dot{V}_f$ is provided during hyro-

dynamic relaxation. It is noteworthy that fractogram 4 appears without a void peak which is commonly found in conventional channel systems in FFF. The conventional systems (symmetrical and asymmetrical channel) mostly generate a void peak which is caused by the following reasons related to the static relaxation process: an abrupt change in system pressure caused when flow directions are altered by valve operations or an unwanted sweep of perturbed sample particles when migration flow is suddenly resumed. Since there is no abrupt change in system pressure or in flow direction during hydrodynamic relaxation, removal or a significant decrease of void peak is one of the advantages of running an FI-AFlFFF channel.

A multi-component separation using an FI-AFlFFF channel is demonstrated with five different polystyrene latex standards and the separation fractogram as shown in Figure 7 is obtained at $\dot{V}_s/\dot{V}_f = 0.1/2.5$ mL/min. and $\dot{V}_{out}/\dot{V}_c = 0.40/2.20$ mL/min by using channel I. Figure 7 shows the capability of the FI-AFlFFF channel system in providing a high resolution separation of nano-particles ranging from 20 nm to 222 nm within 25 minutes. It is clearly shown that particles whose sizes differ about 40 nm from each other are well separated at the baseline resolution. The present run condition is applied for the separation of a polydispersed nano-particle sample. A fumed silica sample purchased from Sigma is tested for the characterization of size and particle size distribution with the current FI-AFlFFF channel system. The fumed silica sample is injected with a diluted suspension and the detector signal for the polydispersed fumed silica is plotted in Figure 8 along with the micrograph of the original sample obtained by field emission SEM. Since the separation of the fumed silica sample is obtained at the same flow rate condition used for obtaining Figure 7, the elution profile of the fumed silica sample can be directly compared for the diameter confirmation. The diameter values correspond to each time scale can be simply calculated by using equation 14 and its scale is marked at the upper axis of the
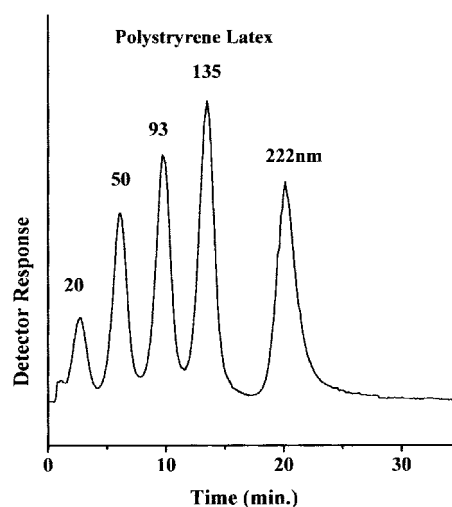

Figure 7. Separation of polystyrene latex standards by FI-AFlFFF using hydrodynamic relaxation obtained at $\dot{V}_s = 0.10$, $\dot{V}_f = 2.5$, $\dot{V}_c = 2.2$, and $\dot{V}_{out} = 0.40$ mL/min.
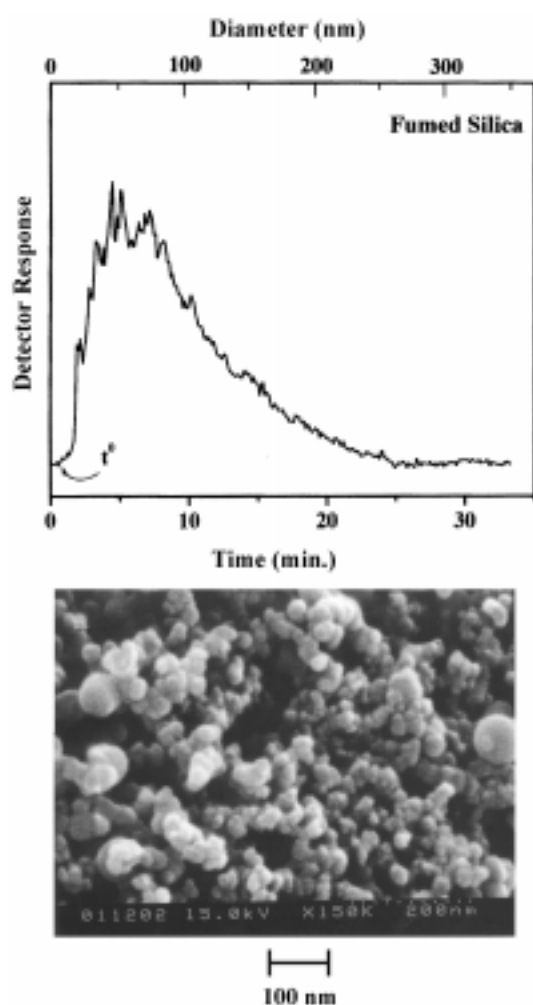
Figure 8. Separation of fumed silica sample by FI-AFlFFF along with the SEM micrograph of the original sample. Run condition is the same as used in Figure 7.

plot in Figure 8 instead of providing a separate plot for particle size distribution. As seen from the figure, the elution profile of the fumed silica sample is very broad and most particles appear to elute within 10 minutes. The corresponding diameter at this time scale is about 100 nm. The microscopic observation of the sample particles shows that a majority of fumed silica particles are smaller than about 60 nm as a primary particle size and a few are nearly 80 nm. It also shows a possibility of containing aggregated particles or fused ones. Since aggregated particles during flow FFF runs are expected to behave as larger particles having an equivalent hydrodynamic volume, they will elute at a longer retention time and the long tailing of peak above 10 min. is expected to be the retention of such aggregated particles or a few large particles. Figure 8 demonstrates the great potential of an FI-AFlFFF system that can be applied powerfully for the separation and size characterization of nanosized materials.

Hydrodynamic relaxation in frit-inlet asymmetrical channels provides an ease in system operations compared to the conventional focusing/relaxation technique since there is no need for valve operations for the flow conversion before and

after relaxation. However, the relaxation efficiency of the focusing/relaxation technique for a conventional asymmetrical channel will be higher than the hydrodynamic relaxation technique since the focusing process compresses the injected sample band into a narrow one which results in the reduction of band broadening of an eluted peak. Retention and efficiency for both relaxation techniques are compared in Figure 9. For the two runs, the same channel system III is used except that the channel depletion wall for a conventional asymmetrical channel is used with a glass plate as found in earlier reports.[11-13] The outflow conditions for the two channels are the same as $\dot{V}_{out}/\dot{V}_c$ =0.20/7.0 mL/min. For the asymmetrical system (run a), channel inlet flow rate is $\dot{V}_{in}$ =7.1 mL/min with an injection flow of 0.1 mL/min. For the frit-inlet asymmetrical system (run b), the rate of injection to frit flow rate is $\dot{V}_s/\dot{V}_f$ =0.20/7.0 mL/min. Since the injection of protein mixtures in the conventional asymmetrical channel is made at 3.0 cm from the channel inlet end, focusing/relaxation is adjusted to take place below the injection point and the protein samples begins to migrate from this point. The reduced migration distance for the asymmetrical channel results in the decrease of retention time for each sample component compared to the other run. In the case of hydrodynamic relaxation using an FI-AFlFFF channel, the elution of each component appears with a substantial increase in retention time. Both systems show an excellence in resolving a broad MW range of proteins, but it is noted that the focusing/relaxation system exhibits a greater efficiency in relaxation with a reduction of peak broadening of
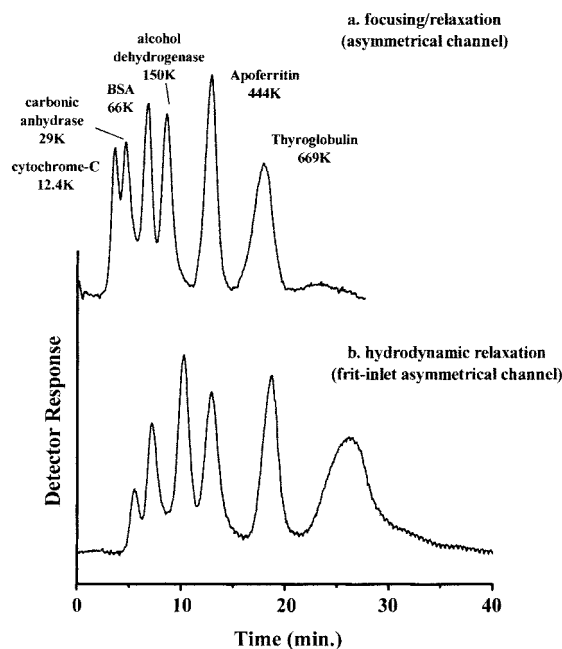

Figure 9. Comparison of separation resolution for protein mixtures obtained by (a) a conventional asymmetrical channel and (b) frit-inlet asymmetrical channel. Outflow conditions are fixed as $\dot{V}_{out}$ = 0.20 and $\dot{V}_c$ = 7.0 for both runs. Injection flow rate and the inlet flow rate ($\dot{V}_{in}$) for run a are 0.10 and = 7.10 mL/min. Focusing point is 3.0 cm from the channel inlet. For run b, $\dot{V}_s$ = 0.20, $\dot{V}_f$ = 7.0 mL/min.
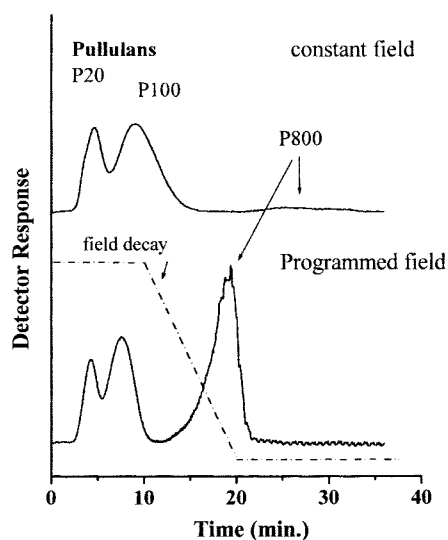
Figure 10. Separation of pullulan standards with constant field operation and with linear field programming by FI-AFlFFF obtained at $\dot{V}_s = \dot{V}_{out} = 0.10$ mL/min. Outflow rate for both runs are the same as $\dot{V}_{out} = 0.10$ mL/min. For the constant field run, $\dot{V}_s$ is maintained at 1.20 mL/min. For the programmed run, $t_1 = 10$ min, $t_p = 10$ min, $\dot{V}_{c0} = 1.20$ mL/min, $\Delta V_c = 1.10$ mL/min.

long retained components such as apoferritin and thyroflo-bulin. However, it is shown that a stopless flow operation in an asymmetrical channel by using a frit inlet can be applied to the separation of proteins.

An FI-AFlFFF system is used to separate water soluble polymers, such as pullulan in Figure 10. Separation of pullulan standards is carried out with or without the application of field programming. Figure 10 compares the difference in peak recovery of pullulan samples before and after the use of field programming. The upper run is made with a constant field condition in which field strength is constantly maintained and the run conditions are $\dot{V}_s/\dot{V}_f = 0.1/1.2$ mL/min. and $\dot{V}_{out}/\dot{V}_c = 0.10/1.2$ mL/min. When an isocratic run condition is used, P20 (Mw=22.8 K) and P100 (Mw=112 K) are resolved well each other but P800 (Mw=788 K) is not recovered at all. Since pullulans are linear polysaccharides, they exhibit less compact conformation than proteins that are rather globular in shape and they tend to diffuse from the channel wall less actively than proteins of the same MW. Therefore, linear polymers require relatively mild field strength for elution. The current field strength condition is too high for P800 to be separated from the other two samples. When field strength is decayed linearly, reduction of retention time is clearly shown with an improved peak recovery in the lower fractogram. For field programming, crossflow rate $\dot{V}_c$ is set so that it equals to the frit flow rate, $\dot{V}_f$, by circulation. An initial delay time, t_1, of 10 minutes is used with the transient time, t_p, of 10 minutes. The crossflow rate decreases from 1.2 to 0.1 mL/min over the transient time period.

In Figure 11, separation of polystyrene sulfonate (PSS) standards of a broad MW range (4 K~1,000 K) are success-fully demonstrated with the aid of field programming. The
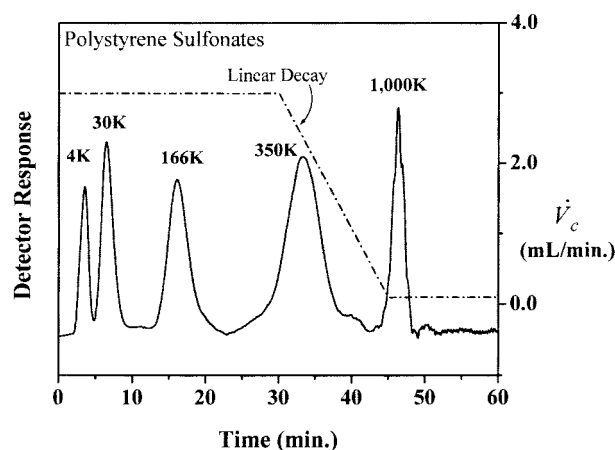

Figure 11. Separation of PSS standards with field programming ($t_1 = 30$ min, $t_p = 15$ min, $\dot{V}_{c0} = 3.0$ mL/min, $\Delta V_c = 2.9$ mL/min) obtained at $\dot{V}_s = \dot{V}_{out} = 0.10$ mL/min. The run is made at $\dot{V}_f = \dot{V}_c$ during programming. System II with YM-10 membrane is used.

run is made with channel II with the initial crossflow rate of 3.0 mL/min. and $\dot{V}_s = \dot{V}_{out} = 0.1$ mL/min. The crossflow rate starts decreasing after 30 minutes of initial delay period to 0.1 mL/min after a 15 minute transient period. In Figure 11 separation is made for the very high MW materials together with low MW materials in the same run. When a constant field condition is used with the crossflow rate of 3.0 mL/min., PSS 1,000 KDa was not seen to elute at all with a relatively broad recovery for PSS 350 KDa and this was not shown in this report. Figure 10 shows the great capability of field programming in an FI-AFlFFF system to separate a wide MW range of water soluble polymers in a single run.

Summary

This article demonstrates that FI-AFlFFF system can be applied for the separation of nanoparticles and macromole-cules without a static relaxation process, such as focusing/relaxation, which is an essential part of the operation in a conventional asymmetrical flow FFF channel. By using a small inlet frit near the channel inlet of an asymmetrical channel, sample materials can be directly injected into the flowing streamline for hydrodynamic relaxation and the separation process begins smoothly without halting the migration flow. For a successful hydrodynamic relaxation in an FI-AFlFFF system, the ratio of sample flow to frit flow must be as small as about 0.05. Since the FI-AFlFFF system operates without stopping the migration flow, the system is much more easily operated compared to the conventional flow FFF systems. The detector signal is relatively stable and the possible sample adsorption onto the channel wall (the membrane) can be reduced to some degree. So far, the complicated flow patterns in an FI-AFlFFF system has been clearly understood and the retention phenomena in the developed system is clearly understood theoretically. The theoretical and experimental evaluations on the FI-AFlFFF system show a great potential in the application of the developed system for the calculation of particle size distribution of

polydisperse particulate materials. In addition, the availability of field programming in FI-AFlFFF system provides a great flexibility for the separation of a broad MW range of polymers and biological macromolecules. Dual field and flow programming can be a good alternative when resolving ultrahigh MW polymers. Further studies are needed for the optimization of the length of the inlet frit for an efficient hydrodynamic relaxation and for a detailed study on the sample recovery for an FI-AFlFFF system.

References

1. *Field-Flow Fractionation Handbook*, Schimpf, M.; Caldwell, K. D.; Giddings, J. C., Eds.; John Wiley & Sons, Inc.: N.Y., 2000.
2. Giddings, J. C. *Science* **1993**, *260*, 1456.
3. Giddings J. C. *Sep. Sci.* **1966**, *1*, 123.
4. Hovingh, M. E.; Thompson, G. E.; Giddings, J. C. *Anal. Chem.* **1970**, *42*, 195.
5. Yang, F. J. F.; Myers, M. N.; Giddings, J. C. *Anal. Chem.* **1974**, *46*, 1924.
6. Ratanathanawongs, S. K.; Giddings, J. C. In *Chromatography of Polymers: Characterization by SEC and FFF*; Provder, T., Ed.: ACS Symposium Ser. 521, ACS: Washington, D.C., 1993; pp 13-29.
7. Lee, S.; Rao, S. P.; Moon, M. H.; Giddings, J. C. *Anal. Chem.* **1996**, *68*, 1545.
8. Benincasa, M. A.; Giddings, J. C. *Anal. Chem.* **1992**, *64*, 790.
9. Ratanathanawongs, S. K.; Giddings, J. C. *Anal. Chem.* **1992**, *64*, 6.
10. Moon, M. H.; Kim, Y. H.; Park, I. *J. Chromatogr. A* **1998**, *813*(1), 91.
11. Wahlund, K.-G.; Giddings, J. C. *Anal. Chem.* **1987**, *59*, 1332.
12. Wahlund, K.-G.; Litzén, A. *J. Chromatogr.* **1989**, *461*, 73.
13. Litzen, A.; Wahlund, K.-G. *Anal. Chem.* **1990**, *62*, 1001.
14. Lee, S.; Myers, M. N.; Giddings, J. C. *Anal. Chem.* **1989**, *61*, 2439.
15. Giddings, J. C. *Anal. Chem.* **1990**, *62*, 2306.
16. Liu, M.-K.; Williams, P. S.; Myers, M. N.; Giddings, J. C. *Anal. Chem.* **1991**, *63*, 2115.
17. Moon, M. H.; Kwon, H. S.; Park, I. *Anal. Chem.* **1997**, *69*, 1436.
18. Moon, M. H.; Kwon, H. S.; Park, I. *J. Liq. Chrom. & Rel. Technol.* **1997**, *20*, 2803.
19. Moon, M. H.; Williams, P. S.; Kwon, H. S. *Anal. Chem.* **1999**, *71*, 2657.
20. Moon, M. H.; Williams, P. S.; Kang, D. Submitted.
21. Giddings, J. C.; Yang, F. J. F.; Myers, M. N. *Anal. Chem.* **1976**, *48*, 1126.
22. Lee, W. J.; Min, B. R.; Moon, M. H. *Anal. Chem.* **1999**, *71*, 3446.
23. Moon, M. H.; Lee, K. H.; Min, B. R. *J. Microcolumn Sep.* **1999**, *11*, 676.
24. Williams, P. S.; Giddings, J. C. *Anal. Chem.* **1987**, *59*, 2038.
25. Kirkland, J. J.; Yau, W. W.; Doerner, W. A.; Grant, J. W. *Anal. Chem.* **1980**, *52*, 1944.
26. Myers, M. N. *J. Microcolumn Sep.* **1997**, *9*, 151.
27. Beckett, R.; Jiang, Y.; Moon, M. H.; Liu, G.; Giddings, J. *Part. Sci. Technol.* **1994**, *12*, 89.
28. Myers, M. N.; Chen, P.; Giddings, J. C. In *Chromatography of Polymers*; Provder, T., Ed.; ACS Symposium Series 521, American Chemical Society: Washington, DC, 1993; pp 47-62.
29. Kirkland, J. J.; Rementer, S. W.; Yau, W. W. *Anal. Chem.* **1981**, *53*, 1730.
30. Yau, W. W.; Kirkland, J. J. *Sep. Sci. Technol.* **1981**, *16*, 577.
31. Giddings, J. C.; Caldwell, K. D.; Moellmer, J. F.; Dickinson, T. H.; Myers, M. N.; Martin, M. *Anal. Chem.* **1979**, *51*, 30.
32. Williams, P. S. *J. Microcol. Sep.* **1997**, *9*, 459.